Strength softening models of soil and its application in rainfall-induced landslide simulation

Zhendong Fu,[a)] and Jiachun Li[b)]
Key Laboratory for Mechanics in Fluid Solid Coupling Systems, Institute of Mechanics, Chinese Academy of Sciences, Beijing 100190, China

(Received 1 July 2013; accepted 2 July 2013; published online 10 July 2013)

Abstract In this study, strength softening models are developed for exploring rainfall-induced landslide mechanism based on Mohr–Coulomb strength theory with both saturation degree and temporal evolution into consideration. According to the ratio of two time scales available, the model can be classified into three categories, i.e., instant softening model, delay softening model, and coupling softening model. Corresponding evolution functions are specified to represent these kinds of softening processes and then applied to simulate landslide of homogeneous slopes triggered by rainfall, therefrom, useful conclusions can be drawn in the end. © *2013 The Chinese Society of Theoretical and Applied Mechanics.* [doi:10.1063/2.1304202]

Keywords: homogeneous slope, numerical simulation, strength softening model, rainfall-induced landslide, geological disaster

Rainfall-induced landslide is a geological disaster of common occurrence all over the world. The great economic losses and casualties in this regard have attracted considerable public attention for decades. The natural landslides are generally the consequence of numerous complex causes including external forcing, slope structure, soil category and initial/boundary states, among which rainfall is usually regarded as a major trigger.[1] During rainfall, overland flow leads to surface soil erosion while rain infiltration results in the rise of perched water table accompanied by growth in pore hydraulic pressure and fall in soil matric suction.[2,3] All of these processes then bring about drop in soil shear strength. If the shear strength at the potential failure surface in the slope decreases to a certain threshold, static equilibrium can hardly be sustained any more, landslide then occurs.

Shallow landslides often occurring during transient rainfall infiltration have attracted extensive interest by numerous researchers. Parametric studies of soil permeability, initial water table, rainfall intensity and duration, etc., were conducted for improving the understanding of rainfall-induced landslide mechanism.[2,4–6] It was found that the metric suction is crucial to the stability of unsaturated soil slopes under rainfall infiltration.[7] Field experiments revealed that the deepening of wetting band along with a lessened matric suction could trigger the failure of a soil slope.[8,9] The magnitude of wetting front suction plays a pivotal role in the stability of slopes in weathered soil. Moreover, the wetting band shall eventually move from shallow to deep layer. Then the infiltration rate can significantly affect the time interval for landslide to initiate. Reduced-scale model tests revealed some mechanism of rainfall-induced failures, especially for sandy slope.[10,11] Under certain circumstances, slopes with non-uniform distributions of soil water content are probably in a critical failure state. The saturation is usually high along the soil-bedrock interface or a relatively impermeable layer.[12] The seepage erosion and resulting unstable zone at the toe account for the start of retrogressive sliding failure of a sandy slope.[13]

On the other hand, theoretical studies as for the stress state in unsaturated soil have also been performed by researchers. In addition to the well-established concept of soil-water characteristic curve (SWCC), a parallel concept of suction stress characteristic curve (SSCC) for unsaturated soil was proposed.[14] Actually, the macroscopic stress called suction stress is generated by mesoscopic inter-particle physicochemical cementation, surface tension force and the force arising from negative pore-water pressure dependent on the degree of saturation. The experiments showed that both Mohr–Coulomb and critical state failures can be accounted for by the SSCC concept. Researchers also proved that the matric suction is a stress state variable rather than a stress variable in unsaturated soil mechanics.[15] These concepts are very helpful for the understanding of evolution process of stress state in unsaturated soil. Numerical model and framework have also been developed to estimate the stability of the slope under steady unsaturated seepage conditions and the occurrence of shallow rainfall-induced landslides.[16,17]

Despite the remarkable progresses in the understanding of rainfall-induced landslide, there are still lots of challenges to be resolved. Firstly, the research on rainfall-induced deep-seated landslides is relatively insufficient compared with the shallow landslides. In addition to the numerous case studies on certain landslide events, theoretical and experimental investigations for universal purpose are absolutely desired for interpreting and forecasting rainfall-induced landslide scale (especially the depth) and moment of occurrence. In other words, we should answer in what condition the rainfall

a) Email: bai_shan_ren@163.com.
b) Email: jcli05@imech.ac.cn.

could induce shallow landslides and in what condition it might trigger deep-seated ones. In particular, traditional studies are usually based on the assumption that the failure takes place along soil-bedrock interface. However, the soil-bedrock interface very probably turns out so deep (tens or hundreds of meters below the ground for deep clay deposits) that the models available are no longer suitable.[12] New theoretical model or experimental analysis for identification of the slip depth is required. Secondly, since the features of soil can affect its permeability, strength, density and other properties, then the reduction of strength with saturation should be a fairly complicated temporal evolution process. Due to the ignorance of this factor, the developed model may cause relatively larger error for predicting the occurrence moment of landslide (7 hours ahead of the observations on average[17]). Hence, the issue of water-soil interaction is really a tremendous challenging to us.

In this study, we have developed a strength softening model for exploring the mechanisms of rainfall-induced landslide based on Mohr–Coulomb strength theory with both saturation and temporal factor taken into consideration. Total and effective stress methods are adopted respectively to deal with unsaturated and saturated zones of the slope. The softening functions for three models have been assumed. Numerical simulation of the landslides demonstrates that the soil strength softening process plays a fundamental role in rainfall-induced landslide and the present model along with reliable material parameters can be used for interpreting and forecasting the scale/depth and occurrence moment of rainfall-induced landslides.

The infiltration of water into soil, especially unsaturated soil, usually leads to the falling of strength. This phenomenon could be attributed to the reduction in matric suction as a result of physical and chemical reaction between water and soil particles, etc. At the same time, the features of soil with pores, fractures and other hierarchical structures are usually very complicated. As a matter of fact, the strength softening should be a temporal evolution process dependent on multifactors. For this reason, we developed here a strength softening model with the consideration of the temporal effect. With other secondary factors ignored, the strength parameter of the soil based on Mohr–Coulomb strength theory should have the following functional forms

$$C = C_0 \cdot f_C(S,t), \tag{1}$$

$$\varphi = \varphi_0 \cdot f_\varphi(S,t), \tag{2}$$

$$\sigma^{\mathrm{t}} = \sigma_0^{\mathrm{t}} \cdot f_\sigma(S,t), \tag{3}$$

where C, φ, and σ^{t} are the cohesion, internal friction angle, and tensile strength of soil, C_0, φ_0, and σ_0^{t} are corresponding values of the original unsaturated soil, t indicates time and S implicitly dependent on t represents the saturation, and f_C , f_φ, f_σ are corresponding softening evolution functions. It should be noted that in the previous studies the time factor is usually neglected where the strength parameters are treated as the functions of saturation only.

There are two different time scales in the present strength softening model, i.e., the time scale of soil saturation variation and the time scale of softening evolution. The strength softening model can be classified into three types according to the ratio of these two time scales.

Instant softening model If the time scale of saturation variation is relatively longer in comparison with that of softening process, then the strength of soil shall vary immediately with saturation. The strength softening model can be treated as instant softening model as illustrated by curve AE in Fig. 1. In this case, the strength parameters are the functions of saturation and the saturation is a function of time. According to the existing experimental data of unsaturated soils about the relationship of strength parameters and its saturation,[18] the evolution function in this model may be assumed to be

$$C_{AE}(S) = \begin{cases} C_0\left(A_C + B_C \cdot \mathrm{e}^{C_c S(t)}\right), & 0 < t \leqslant t_i, \\ C_0\left(A_C + B_C \cdot \mathrm{e}^{C_c S_i}\right), & t_i < t, \end{cases}$$

$$\varphi_{AE}(S) = \begin{cases} \varphi_0\left(A_\varphi + B_\varphi\, S(t)\right), & 0 < t \leqslant t_i, \\ \varphi_0\left(A_\varphi + B_\varphi\, S_i\right), & t_i < t, \end{cases} \tag{4}$$

$$\sigma^{\mathrm{t}}_{AE}(S) = \begin{cases} \sigma^{\mathrm{t}}_0\left(A_C + B_C \cdot \mathrm{e}^{C_c S(t)}\right), & 0 < t \leqslant t_i, \\ \sigma^{\mathrm{t}}_0\left(A_C + B_C \cdot \mathrm{e}^{C_c S_i}\right), & t_i < t. \end{cases}$$

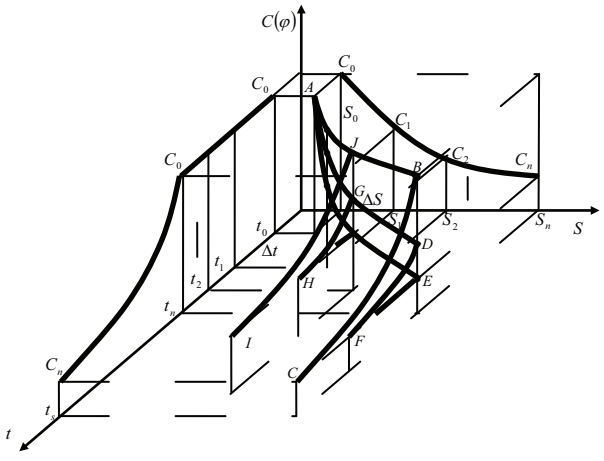

Fig. 1. Schematic diagram of strength softening model.

The cohesion and tensile strength vary exponentially while the internal friction angle changes linearly. The functions in parentheses are normalized as dimensionless evolution functions while A_C, B_C, C_C and A_φ,

B_φ are the parameters in these softening functions determined by soil test. And t_i is the moment when the saturation stops changing. In-cohesive or slightly cohesive coarse-grained soil, expansive soil, collapsible loess, etc., may exhibit instant softening characteristics.

Delay softening model Secondly, if the time scale of saturation variation is relatively shorter in comparison with that of softening process, then the soil strength shall still vary slowly with time at a certain saturation degree. The strength softening model can be treated as delay softening model as illustrated by curve ABC in Fig. 1. Then the evolution functional specified of this model is assumed as

$$
\begin{aligned}
&C_{ABC}(S) = \\
&\quad\begin{cases} C_0,\ 0 < t \leqslant t_0, \\ C_0\big[A_C^n + B_C^n \cdot \mathrm{e}^{C_C^n(t-t_0)}\big],\ t_0 < t \leqslant t_s, \\ C_{AE}(S_i),\ t_s < t, \end{cases} \\
&\varphi_{ABC}(S) = \\
&\quad\begin{cases} \varphi_0,\ 0 < t \leqslant t_0, \\ \varphi_0\left[A_\varphi^n + B_\varphi^n \cdot \mathrm{e}^{C_\varphi^n(t-t_0)}\right],\ t_0 < t \leqslant t_s, \\ \varphi_{AE}(S_i),\ t_s < t. \end{cases}
\end{aligned} \tag{5}
$$

We assume here that all the strength parameters vary exponentially with time while A_C^n, B_C^n, C_C^n and A_φ^n, B_φ^n, C_φ^n are parameters of the softening functions determined by soil test, where the superscript "n" denotes delay or non-instant model. Generally speaking, these parameters should depend on the present saturation of soils, i.e., S_i and the functional forms of the softening process should also be determined by soil tests. t_0 are the moment when the softening process starts and t_s is the moment while the strength stops changing. The soil may own the delay softening properties if the physical-chemical reaction and erosion play an important role in the variation of strength.

Coupling softening model If the time scales of saturation variation and softening evolution are the same order of magnitude, then the strength of soil shall vary with both saturation and time. The strength softening model can be treated as coupling softening model as illustrated the curve ADF in Fig. 1. The evolution function of this model reads

$$
\begin{aligned}
&C_{ADF}(S) = \\
&\quad\begin{cases} C_0\left(A_C + B_C \cdot \mathrm{e}^{C_C S(t)}\right),\ 0 < t \leqslant t_0, \\ C_0\left(A_C + B_C \cdot \mathrm{e}^{C_C S(t)}\right) \cdot \\ \qquad \left[A_C^n + B_C^n \cdot \mathrm{e}^{C_C^n(t-t_0)}\right],\ t_0 < t \leqslant t_s, \\ C_{AE}(S_i),\ t_s < t, \end{cases} \\
&\varphi_{ADF}(S) = \\
&\quad\begin{cases} \varphi_0\left(A_\varphi + B_\varphi S(t)\right),\ 0 < t \leqslant t_0, \\ \varphi_0\left(A_\varphi + B_\varphi \cdot \mathrm{e}^{C_C S(t)}\right) \cdot \\ \qquad \left[A_\varphi^n + B_\varphi^n \cdot \mathrm{e}^{C_\varphi^n(t-t_0)}\right],\ t_0 < t \leqslant t_s, \\ \varphi_{AE}(S_i),\ t_s < t. \end{cases}
\end{aligned} \tag{6}
$$

These evolution functions evidently consist of two parts, i.e., the instant softening component and the delay softening component. The residual strength of the instant softening component is an important factor for the coupling softening model. The cohesion varies exponentially with both time and saturation while the internal friction angle varies linearly with saturation and exponentially with the time variable. The tensile strength possesses the same functional form as cohesion just with C_0 replaced by σ_0^{t}. In the evolution functions, A_C, B_C, C_C, A_φ, B_φ and A_C^n, B_C^n, C_C^n, A_φ^n, B_φ^n, C_φ^n are parameters of the softening functions determined by soil test. Generally, the parameters $A_\varphi^n - C_\varphi^n$ should depend on the present saturation of soils, i.e., they are functions of S_i. The soil which own complicated structures and feature such as pores, fissures, cementation, dissolution, etc., may display the coupling softening property.

We use the proposed strength softening model to simulate the rainfall-induced landslide of a homogeneous slope. The simplified numerical model in the vertical plane is shown in Fig. 2. The composition of a slope is formed by homogeneous unsaturated soils. In the standard numerical example, the boundary conditions of the soil skeleton and fluid are as follows. We specify fixed boundary condition at the slope bottom and free boundary condition at the top. In contrast, the left and right sides are all horizontally fixed and vertically free. At the same time, the hydraulic pressure at the top maintains a fixed value without additional other fluid dynamic conditions are otherwise imposed. Moreover, transverse soil skeleton size in y–direction for a two dimensional slope is usually assumed as 1 m and the displacement in this direction vanishes in all computations.

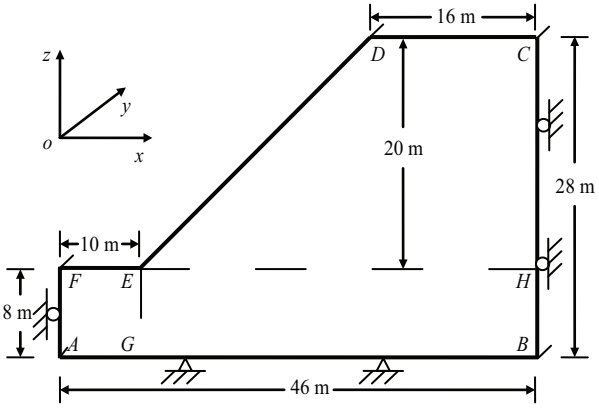

Fig. 2. Simplified numerical model for rainfall-induced landslide simulation.

The simulation of rainfall-induced landslide is presented in FLAC^{3D} Version 3.00.[19] The parameters that can be useful in computation are adopted as below: the dry density of soil $\rho^{\mathrm{d}} = 2.0 \times 10^3\,\mathrm{kg/m^3}$, the bulk and shear modules of soil skeleton $K = 100$ MPa and $G = 30$ MPa, the cohesion prior to and after softening $C_0 = 0.1$ MPa and $C_n = 20\,\mathrm{kPa}$, the tensile strength prior to and after softening $\sigma_0^{\mathrm{t}} = 0.1$ MPa and $\sigma_n^{\mathrm{t}} = 20$ kPa, the internal friction angles prior to and after softening $\varphi_0 = 20^\circ$ and $\varphi_n = 5^\circ$, the isotropic permeability of the saturated soils $k = 0.5\,\mathrm{m^2/(GPa \cdot s)}$, the reduction factor of permeability for unsaturated soils $k^{\mathrm{rw}}(S) = S^2(3-2S)$, the bulk modulus of water $K_{\mathrm{w}} = 2.0$ GPa, the porosity $n = 0.2$, the original saturation of unsaturated soil $S_0 = 0$, the tensile strength of water $\sigma_{\mathrm{w}}^{\mathrm{t}} = 10\,\mu\mathrm{Pa}$, the density of water $\rho^{\mathrm{w}} = 10^3\,\mathrm{kg/m^3}$, the acceleration of gravity $g = 9.8\,\mathrm{m/s^2}$. The above parameters may correspond to natural consolidated clays.

In the following standard numerical examples, the parameters in evolution function are given as follows. The time-related softening process starts at $t_0 = 1$ h and lasts for 3 hours, while the residual strength of the instant softening component is 60% of the original values for coupling softening model. For strength parameters, i.e., C_0 and C_n, φ_0 and φ_n, σ_0^t and σ_n^t given above, the parameters can then be calculated by numerical fitting. Take evolution function (4) as an example, if $S = 0$, then we have $A_C + B_C = 1.0$. If $S = 1$, then we have $A_C + B_C \cdot \mathrm{e}^{C_C} = C_n/C_0$. If we specify two values of the three parameters, for example $A_C = 0.1$ and $B_C = 0.9$, then we will get $C_C = -2.197\,2$. In this manner, the parameters in evolution function (4) are chosen as $A_C = 0.1, B_C = 0.9, C_C = -2.197\,2, A_\varphi = 1.0, B_\varphi = -0.75$. The parameters in evolution function (5) are specified as $A_C^n = 0.1, B_C^n = 0.9, C_C^n = -0.732\,4, A_\varphi^n = 0.1, B_\varphi^n = 0.9, C_\varphi^n = -0.597\,2$. The parameters in evolution function (6) are assumed to $A_C = 0.1, B_C = 0.9, C_C = -0.587\,8, A_C^n = 0.1, B_C^n = 0.9, C_C^n = -0.450\,0, A_\varphi = 1.0, B_\varphi = -0.4, A_\varphi^n = 0.1, B_\varphi^n = 0.9, C_\varphi^n = -0.348\,2$. If necessary, additional parameters and conditions will be promptly given.

The mesh discretization scheme of the simplified numerical model (as shown in Fig. 2) is 5×4 (AGEF) + 18×4 (GBHE) + 18×16 (EHCD). There is only one layer grid cell in y-direction. Under these conditions given above, the safety factor of the slope calculated by the strength reduction method[20] is 2.33 for the original unsaturated state and 0.49 for the fully saturated state after the softening process. The simulation of rainfall-induced landslide is presented in FLAC^{3D} Version 3.00.[19] Firstly, the initial ground stress is calculated in non-CONFIG fluid mode. Then the coupled fluid flow-mechanical calculation is carried out in CONFIG fluid mode. The mechanical calculation is identified as the slave component in the fluid flow-mechanical process, while the fluid module is declared as the master.

Example 1 For the first numerical example, the instant softening model is used to simulate the landslide processes trigged by rainfall. The hydraulic pressure at the top side of the numerical model maintains 10 Pa to simulate heavy rain conditions. Water infiltration into slope is mainly due to gravity from the initial unsaturated state. Point D in Fig. 2 is used for monitoring. The landslide starts when the displacement of point D reaches 0.1 m until 0.2 m when the simulation is stopped.

The parameter study with permeability $5.0\,\mathrm{m^2/(GPa \cdot s)}$, $0.1\,\mathrm{m^2/(GPa \cdot s)}$, and $0.5\mathrm{m^2/(GPa \cdot s)}$ is firstly performed in numerical simulations. The results show that for the instant softening model, the permeability only influences the time interval from 1.408 h to 7.042 h when the landslide occurs without affecting the scale of landslide of a certain slope. Namely, the larger the permeability is, the time interval for the landslide to occur the shorter.

The residual strength after softening process is an important factor as well. Three different residual strength are tested, i.e., $C_n = 40\,\mathrm{kPa}$ and $\varphi_n = 8.0^\circ$, $C_n = 30\,\mathrm{kPa}$ and $\varphi_n = 6.0^\circ$, $C_n = 20\,\mathrm{kPa}$ and $\varphi_n = 5.0^\circ$. The results show that larger residual strength might induce larger scale of landslide as illustrated in Fig. 3. Moreover, the landslide depth becomes smaller when the slope becomes steeper.

Example 2 In this example, the delay softening model is used to simulate the landslide processes trigged by rainfall. All the other conditions are kept the same as Example 1.

The effect of permeability for landslide is also examined. Three different values representing high, medium and low permeability respectively are tested, i.e., $10\,\mathrm{m^2/(MPa \cdot s)}$, $0.5\,\mathrm{m^2/(GPa \cdot s)}$, and $0.25\,\mathrm{m^2/(GPa \cdot s)}$. Unlike the instant softening model, permeability has an influence on both the time interval when the landslide occurs and the scale of landslide. For the above three values, the time interval needed are 3.111 h, 3.570 h, 3.995 h and the landslide depths increase with the permeability (as shown in Fig. 4).

The duration of softening process is also an important factor for the delay softening model. In the numerical tests, 2 h, 3 h, and 5 h of softening process are numerically tested, showing that both the landslide time interval and depth increase with the duration of softening process. The landslide time intervals are 2.970 h, 3.570 h, and 4.547 h.

Example 3 In this example, we use the coupling softening model to simulate the landslide processes trigged by rainfall.

The permeability has a significant impact on both time interval and scale/depth of landslide for coupling softening model. For the considered three different permeability values, i.e., $0.25\,\mathrm{m^2/(GPa \cdot s)}$, $0.5\,\mathrm{m^2/(GPa \cdot s)}$, and $10\,\mathrm{m^2/(MPa \cdot s)}$, the landslide depth increases obviously with permeability (as shown in Fig. 5) and the landside time intervals are 3.775 h, 3.079 h, and 2.501 h.

Like the delay softening model, the duration in the delay softening component of the coupling softening model also has an impact on both the landslide time interval and the scale. The scale of landslide for slow softening process is larger than that for fast softening

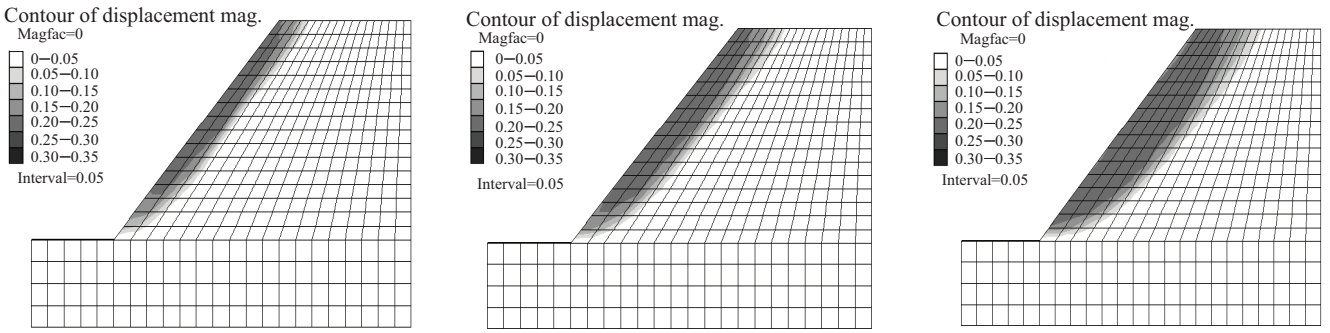

(a) Low residual strength (b) Medium residual strength (c) High residual strength

Fig. 3. The displacement fields (m) of slope under different residual strengths for instant model.

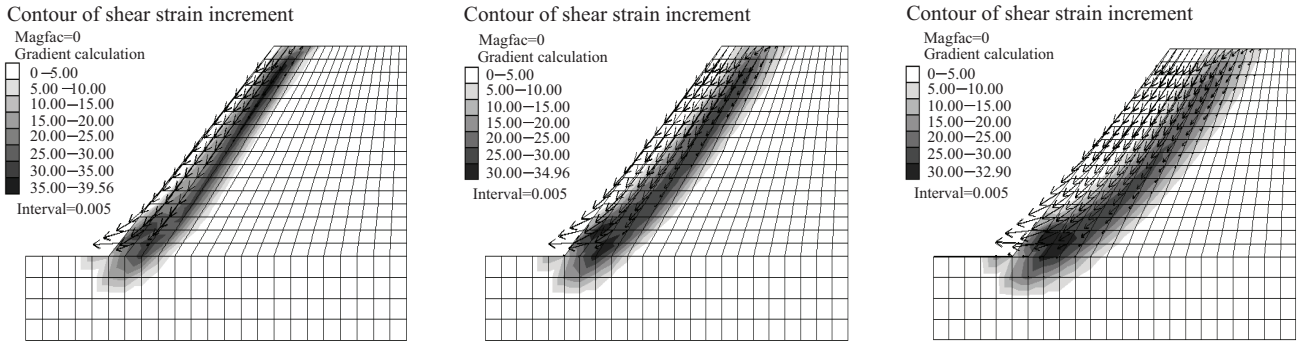

(a) Low permeability (b) Medium permeability (c) High permeability

Fig. 4. Shear bands and displacement vectors of slope for different permeability for delay model.

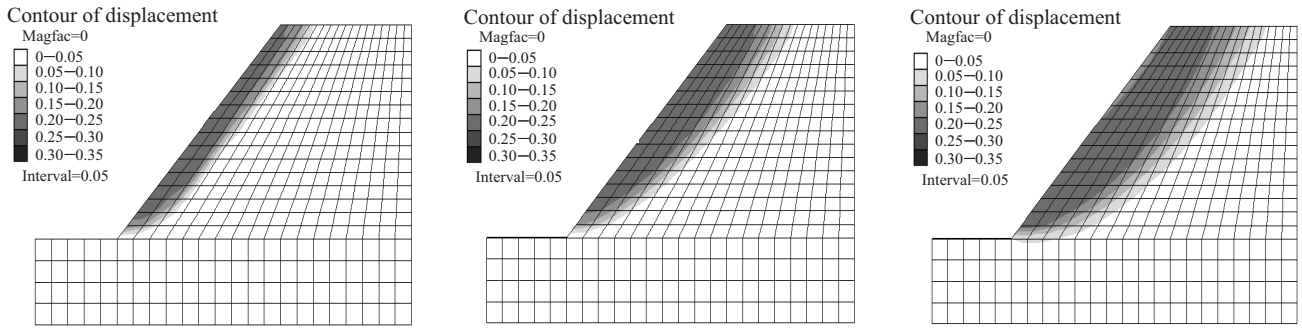

(a) Low permeability (b) Medium permeability (c) High permeability

Fig. 5. The displacement fields (m) of slope for different permeability for coupling model.

process. Moreover, the landslide time interval increases with the duration of the delay softening component in the coupling softening model.

The cases with residual strengths 40%, 60%, 80% of the original unsaturated soil are tested. It is obvious that if the residual strength of the instant softening component is 100% of the original strength, the coupling softening model shall degenerate to the delay softening model. If the residual strength is much weaker such as 20% (cohesion) and 25% (internal friction angle) of the original strength, the coupling softening model shall degenerate to the instant softening model (for the parameters given above). Numerical results show that the landslide time interval monotonically increases with the residual strength of the instant softening component while the scale of the landslide firstly increases and then decreases with it. The landslide time intervals calculated are 2.342 h, 3.079 h, 3.427 h.

Strength softening model of soils is developed in the present study and applied for the simulation of rainfall-induced landslide. The model is based on Mohr–Coulomb strength theory with both saturation degree

and temporal evolution taken into consideration. According to the ratio of two different time scales, i.e., the time scale of saturation variation and the time scale of softening evolution, the model is classified into three types. They are the instant softening type, the delay softening type, and the coupling softening type.

Parameter influence study on permeability, softening duration, and residual strength are conducted for three models, showing that they exert different effects on both the scale/depth and the time interval when the rainfall triggered landslide occurs. Numerical results further demonstrate that the temporal factor should not be ignored in understanding the mechanism of rainfall-induced landslide. In particular, we should notice their respective evolution behaviors of three models with distinct characters. Anyway, the present preliminary study has opened a scope of further exploration in the future.

This work was supported by the National Natural Science Funds of China (10932012).

1. G. Sorbino and M. V. Nicotera, Engineering Geology, http://dx.doi.org/10.1016/j.enggeo.2012.10.008.
2. C. W. W. Ng and Q Shi, Computers and Geotechnics **22**, 1 (1998).
3. P. V. Lade, Engineering Geology **114**, 57 (2010).
4. A. Rahimi, H. Rahardjo, and E.-C Leong, Engineering Geology **114**, 135 (2010).
5. C.-C. Huang and S.-C. Yuin, Geomophology **120**, 326 (2010).
6. I. Egeli and H. F. Pulat, Scientia Iranica **18**, 1179 (2011).
7. D. G. Fredlund and H. Rahardjo, *Soil Mechanics for Unsaturated Soils* (John Wiley & Sons, New York, 1993).
8. X. B. Tu, A. K. L. Kwong, F. C. Dai, et al., Engineering Geology **105**, 134 (2009).
9. J. Kim, S. Jeong, S. Park, et al., Engineering Geology **75**, 251 (2004).
10. C.-C. Huang, C.-L. Lo, J.-S. Jang, et al., Engineering Geology **101**, 134 (2008).
11. C.-C. Huang, Y.J. Ju, L. K. Hwu, et al., Journal of Hydrology **370**, 39 (2009).
12. M. Bittelli, R. Valentino, F. Salvatorelli, et al., Geomorphology **173–174**, 161 (2012).
13. S. D. N. Lourenco, K. Sassa, and H. Fukuoka, Geomorphology **73**, 115 (2006).
14. N. Lu and W. J. Likos, Journal of Geotechnical and Geoenvironmental Engineering **132**, 131 (2006).
15. N. Lu, Journal of Geotechnical and Geoenvironmental Engineering **134**, 899 (2008).
16. N. Lu and J. Godt, Water Resources Research **44**, W11404 (2008).
17. R. L. Baum, J. W. Godt, and W. Z. Savage, Journal of Geophysical Research **115**, F03013 (2009).
18. Z.-Y. Xiao, C.-F. Chen, and J.-X. Yang, Natural Sciences **37**, 20 (2010).
19. Fast Language Analysis of Continua in 3 Dimensions (FLAC3D), Version 3.0 (Itasca Consulting Group, Inc., 2005).
20. E. M. Dawson, W. H. Roth, and A. Drcscher, Geotechnique **49**, 835 (1999).